Hexagonal vortices enable faster colloidal crystal grain coarsening

Helen K. Chaffee,* Eric Corona-Oceguera,* Chris G. Couto,* Avani N. Anne, Elizabeth L. Rogers, Aaron L. Galper, Conor M. Floyd, Ananya Venkatachalam, and Sharon J. Gerbode†
Department of Physics, Harvey Mudd College, Claremont, California 91711, USA

(Received 10 November 2023; accepted 25 June 2024; published 24 July 2024)

We find that localized rotations of hexagonal clusters of particles occur during rapid dissolution of grain boundary loops in two-dimensional colloidal crystals. These particle vortices, or rotating "granules," are distinct from established models for grain boundary diffusion, which predict that a crystal grain enclosed within another crystal will dissolve at a constant rate. Our measurements of colloidal crystal experiments and Brownian dynamics simulations reveal grain boundary motion that is described by two distinct processes: slow dissolution due to the diffusion of individual particles, and rapid dissolution due to collective granule rotation. In the latter process, hexagonal clusters of particles rotate together in granules whose shape and position are determined by the underlying moiré pattern. Furthermore, these vortices guide cooperative strings of particles that move along the edges of the hexagonal granules. Including this vortex mechanism may improve models for grain coarsening in polycrystalline materials, ultimately offering improved predictions for the time evolution of material properties.

DOI: 10.1103/PhysRevE.110.014608

I. INTRODUCTION

Most crystalline materials are polycrystalline, containing many crystal grains separated by disordered interfaces called grain boundaries. Grain boundaries critically influence material properties ranging from yield strength to electrical conductivity [1–3]. Experimental studies of grain boundaries in colloidal crystals have provided insights into physical phenomena such as thermal grain boundary fluctuations [4,5], responses to macroscopic mechanical perturbation [6,7], and the kinetics of grain rotation [8–10]. Established continuum theories for grain boundary motion treat grain boundaries as continuous surfaces (in 3D crystals) or curves (in 2D crystals) that disrupt the local order of the crystal and therefore cost the system free energy [11–14]. Consequently, in two dimensions a grain boundary loop that completely encloses a crystal grain within a surrounding crystal is predicted to shrink at a constant rate so that the number of particles in the grain decreases linearly in time [12,13,15–17]. Moreover, the grain dissolution is predicted to occur via the diffusion of individual particles or atoms across the grain boundary [15,16,18,19], or via rotation of the entire inner grain until it matches the orientation of the outer grain [20–27].

Our colloidal experiments and simulations demonstrate that grain dissolution occurs via two distinct processes, one with individual particle diffusion, and another that is characterized by vortices of hexagonal particle clusters, or "granules," that rotate to switch from one grain to another. We observe that granule rotation is a common event in the motion of a grain boundary loop, and we find that the event is correlated with rapid dissolution of the grain boundary. During granule rotation, particles undergo cooperative rearrangements that are guided by the underlying hexagonal moiré pattern formed by the two lattices that share the grain boundary. The incorporation of granule rotation into models of grain boundary motion could improve predictions of grain coarsening and deliver more accurate expectations for how polycrystalline materials perform.

II. COLLOIDAL EXPERIMENTAL METHODS

We prepare monolayer colloidal polycrystals using 1.3-μm-diameter silica spheres (Sekisui Micropearl Spacers, Dana Enterprises International, CA) suspended in dimethyl sulfoxide. We contain the suspension in a sealed wedge-shaped glass cell as previously described [28] and tilt the cell to allow the particles to sediment into the gap, where they form a crystalline monolayer. To create grain boundary loops within the crystalline monolayers, we use the "optical blasting" technique, described previously in Refs. [10,29]. Briefly, because the refractive index of the particles is less than that of the suspending fluid, a standard optical tweezer setup (800 mW, 1064-nm-laser focused through a 100X Zeiss Plan-Apochromat objective) repels the particles, which move radially outward from the laser axis while remaining in the monolayer. We use optical blasting to create space that then attracts grain boundaries [29]. By repeatedly using optical blasting near an existing grain boundary, we create a bulge and ultimately detach it to generate a grain boundary loop that is disconnected from other grain boundaries.

We characterize local crystal orientation using the order parameter $\Psi_6 = \frac{1}{N}\sum_n e^{6i\Theta_n}$, where the sum is taken over a particle's N nearest neighbors, and Θ_n is the angle between the nth neighbor separation vector and the horizontal axis

*These authors contributed equally to this work.
†Contact author: gerbode@hmc.edu

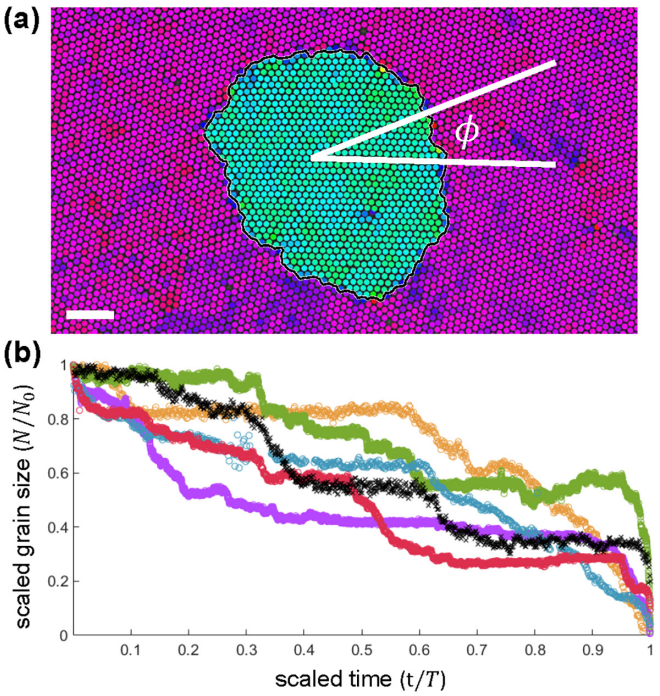

FIG. 1. Dissolution of experimental grain boundary loops. (a) A micrograph of a typical grain boundary loop. Each colloidal particle is colored by local crystal orientation, quantified by the phase of Ψ_6, and ϕ denotes the misorientation angle between the inner and outer grain. Color scale: red–purple is max–min of range. Scale bar: 10 μm. (b) Scaled grain size vs scaled time for multiple experiments. Notably, the dissolution curves do not collapse onto a single line. Each follows a distinct sequence of slow dissolution plateaus and steps. The data shown with black X-shaped markers comes from a naturally occurring grain, while the others are from grains created using optical blasting.

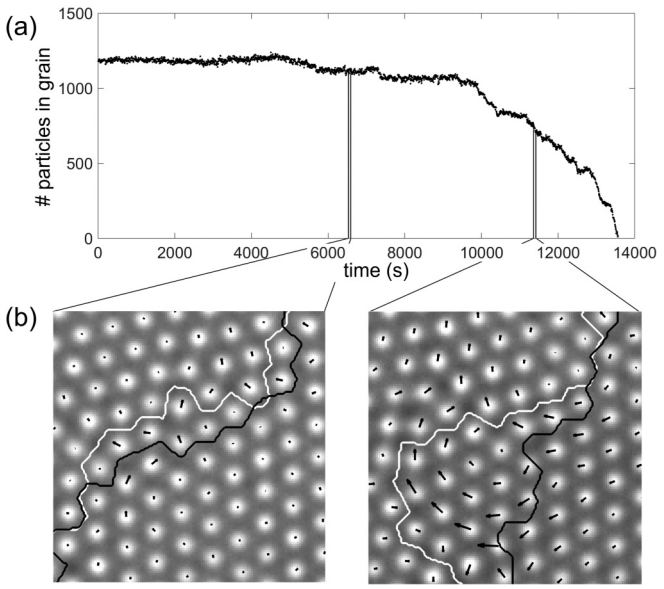

FIG. 2. Plateaus and steps within a single grain dissolution experiment correspond to qualitatively different types of particle displacements. (a) The number of particles in the inner grain over time decreases in slow plateaus and fast steps. (b) Both lower panels show particle displacements over a 1-min interval, but organized particle cluster rotations only occur in the right panel. The location of the grain boundary at the start of the 1-min interval is shown in white, and the final grain boundary is shown in black.

[30]. Each particle's nearest neighbors are determined using Delaunay triangulation. In Fig. 1(a) the color of the ith colloidal particle indicates the phase ψ_i of the local $\Psi_6(i)$, which is averaged over the ith particle and its nearest neighbors. Variations in local orientation show up as color modulations, which are clearly visible both inside and outside of the grain boundary loop, which is shown in black [Fig. 1(a)]. Furthermore, although we attempt to create initially circular grains, thermal fluctuations roughen and reshape the grains even as they form during optical blasting. This is distinct from the perfectly circular grain boundary loops previously created in colloidal experiments by rotating a block of particles using optical tweezers [8,9]. To locate grain boundaries within experimental images, we model the polycrystal as a graph, with each colloidal particle as a vertex connected to its nearest neighbors with edges, and then partition the graph using a minimum cut algorithm to identify separate grains [10].

In total, we observed 16 grain boundary loops, of which two were naturally occurring and the others were created using optical blasting. No qualitative difference was observed between experiments involving grains that formed naturally and those that were fabricated. All loops were disconnected from any other grain boundaries. The enclosed "inner" grains varied in initial size within the range of approximately 200–3000 colloidal particles, and the initial misorientation angles varied between 12° and 29° (note that in a triangular crystal, the maximum misorientation angle is 30°). Each grain boundary loop was observed until it fully dissolved, a process we call "grain dissolution," with dissolution durations, or "grain lifetimes," ranging between about 30 min and 6 h. A table of the experimental data is provided as Table S1 in the Supplemental Material [31].

III. GRAIN DISSOLUTION EXPERIMENTS

In our colloidal experiments, we find that the number of particles in the inner grain does not decrease linearly in time. Indeed, we find that grain dissolution occurs via steplike sequences characterized by plateaus when grain size slowly decreases, punctuated by rapid drops (or sometimes increases) in grain size. Figure 1(b) shows six experimental datasets of the scaled grain size N/N_0 plotted against the scaled time t/T, where N is the number of particles in the inner grain at time t, N_0 is the initial number of particles in the inner grain, and T is the grain lifetime. Notably, when scaled in this way, the curves do not collapse onto a single line, but instead, each has a distinct pattern of plateaus and steps.

We find that the plateau and step regimes of grain dissolution are correlated with two distinct particle-scale mechanisms. As shown in Fig. 2, the slowly sloping plateaus are characterized by the random diffusion of individual particles along and across the grain boundary, while the rapid steps occur when larger clusters of particles cooperatively rotate to switch from the inner grain orientation to the outer. Both of the lower panels of Fig. 2 show particle displacements

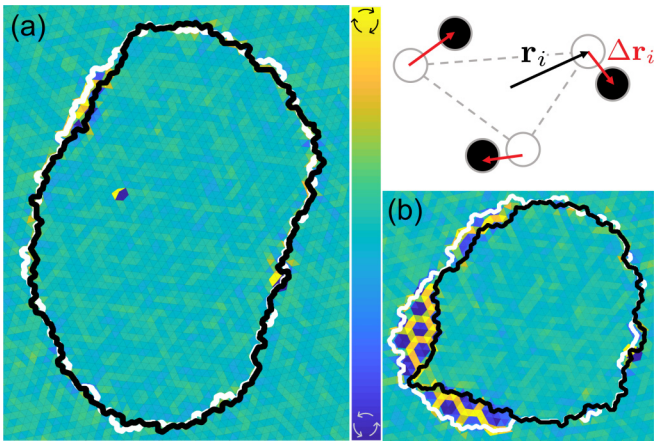

FIG. 3. Vorticity highlights granule rotations during rapid drops in grain size. Inset: Vorticity is calculated for each triangle of the Delaunay triangulation of particle positions as $\mathbf{v} = \sum \mathbf{r}_i \times \Delta\mathbf{r}_i$. (a) A crystal grain shrinking over a 1-min interval, with initial grain boundary (white) and final grain boundary (black) plotted over vorticity color map with clockwise (counterclockwise) vorticity indicated by yellow (blue). Over this plateaulike interval, there are not hexagonal vortices. (b) The same crystal grain shrinking over a different 1-min interval during a more rapid drop in grain size. Here a clear hexagonal pattern emerges in the vorticity.

over a time interval of 1 min. In Fig. 2(a) a few individual particles diffuse across the grain boundary, and there is no clear pattern in their displacements. However, in Fig. 2(b) the particle displacements are arranged in orderly circulation, indicating clusters of particles rotating together.

IV. VORTICITY

To distinguish between the two observed mechanisms of grain boundary motion, we measure the local vorticity in the particle displacement field as $\mathbf{v} = \sum \mathbf{r}_i \times \Delta\mathbf{r}_i$, as defined in [32]. As depicted in the inset of Fig. 3, the sum is over three initially adjacent particles whose positions form the vertices of a triangle; $\mathbf{r}_i$ is the vector from the center of the triangle to the ith initial particle position, and $\Delta\mathbf{r}_i$ is the displacement of the ith particle over a time interval Δt. Typical time intervals range from 15 s to 2 min. We define vortices that point into the page (i.e., clockwise) as positive, and use the magnitude and sign of the vorticity as a color map for each triangular region bounded by particles in our system (Fig. 3). The vorticity color map reveals hexagon-shaped vortices during steps in grain size. The vortices in Fig. 3(b) comprise clusters or "granules" of particles cooperatively rotating counterclockwise, surrounded by outlines of clockwise rotation due to the relative motion of adjacent vortices. By contrast, during the plateaus in grain size, particle motion is not organized into such vortices but instead proceeds through random particle diffusive motion near the grain boundary, as shown in Fig. 3(a).

The rotation of individual granules generally proceeds in one sense, e.g., counterclockwise in Fig. 3(b), causing the inner grain to shrink. However, we also occasionally observe granule rotation in the opposite direction, causing the inner grain to grow (see Supplemental Material, Fig. S1 [31]). These

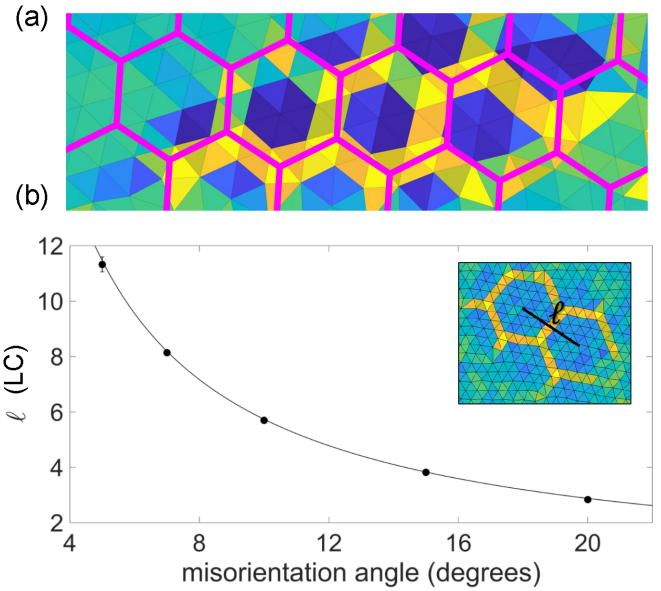

FIG. 4. Rotating hexagonal granules are defined by the underlying moiré pattern. (a) Hexagonal pattern in vorticity data from colloidal experiments is overlaid with a moiré pattern (pink) determined from the lattices of the inner and outer grains' crystal orientations. (b) Granule size, measured as center-to-center spacing in lattice constants (LC) in Brownian dynamics simulations of grain dissolution, decreases with misorientation angle following the prediction (solid line) based on the underlying moiré pattern. Error bars indicate the standard error of the mean.

clockwise and counterclockwise granule rotations are respectively reminiscent of the "couple grain boundary migration" and "grain boundary sliding" mechanisms that have been previously explored in [27]. Here, the locking of crystal rows in the former and sliding of crystal rows in the latter occur at the boundaries of the granules rather than at the boundary of the shrinking grain.

V. MOIRÉ PATTERN

The characteristic hexagonal shape of the rotating granules directly reflects the underlying moiré pattern that can be conveniently visualized by overlaying the crystal lattice of the inner grain with that of the outer grain. As described previously [10], the centers of the hexagonal regions in the moiré pattern are spaced by a distance ℓ according to the misorientation angle ϕ between the two lattices as $\ell = [2\sin(\phi/2)]^{-1}$, measured in units of lattice constants (LCs). To verify that the observed hexagonal vortices align with the moiré pattern, we determine the best-fit triangular lattices to match the crystal orientation of the inner and outer grains, and overlay those lattices to determine the bounds of the moiré pattern hexagons. The result of this is shown as pink hexagonal outlines in Fig. 4(a).

We further confirm the role of the moiré pattern in dictating the shapes and positions of the rotating granules using results from Brownian dynamics simulations. We simulate systems of approximately 25000 particles interacting as hard Brownian disks as previously described [29], and initialize the particles in two crystal grains as in the experiments: one "inner grain"

completely enclosed within a larger "outer grain." During the simulation, the inner grain dissolves until ultimately the entire system has a single-crystal orientation matching that of the outer grain. As in the colloidal experiments, we observe hexagonal patterns in the vorticity of particle displacements during portions of the grain dissolution. We systematically vary the misorientation from 5° to 20° and observe particle displacements over the first 500 frames to identify hexagonal vortices. We measure the spacing ℓ between centers of adjacent hexagonal granules and find that these follow the prediction based on the moiré pattern, with zero fitting parameters [Fig. 4(b)].

Due to the finite size of individual particles in the crystal, there is a lower limit to the size of hexagonal granules. The smallest granule centered on a particle contains seven particles and is spaced by a distance of $\sqrt{7}$ lattice constants from the adjacent granule. This corresponds to a misorientation angle of approximately 22 degrees. Indeed, we have not observed clear, recognizable hexagonal vortices in experiments or simulations with misorientation angles above this value.

Our observation of hexagonal granule rotation fits into the context of other recent studies of grain loops in colloidal crystals, particularly [9], which investigates a critical grain radius R_* for a given misorientation angle ϕ below which the grain rotates rigidly to snap into alignment with the surrounding crystal. This collective grain rotation is reminiscent of the cooperative granule rotation we have observed. In fact, there is a direct relationship between the granule size and the minimum critical size found in [9]. The latter was determined by finding the minimum grain radius that would allow for six dislocations to be spaced by the predicted average distance between dislocations in low-misorientation grain boundaries, which is $1/\phi$ in units of lattice constants. Equating $2\pi R_*/6 = 1/\phi$ results in the minimum critical size $R_* = 3/(\pi\phi)$. For low misorientation angles, the granule size $\ell = [2\sin(\phi/2)]^{-1}$ reduces to $1/\phi$, i.e., the mean distance between dislocations. The relative difference between ℓ and $1/\phi$ is $<1\%$ for all misorientation angles up to the maximum value of 30°. Thus, the minimum critical size from Ref. [9] can be written as $R_* = 3\ell/\pi$. That is, the minimum critical grain size is directly proportional to the size of the hexagonal granules determined by the underlying moiré pattern, hinting that such grains may rotate rigidly because they cannot split into multiple smaller granules.

VI. COOPERATIVE MOTION DURING GRANULE ROTATION

Cooperative motion, in which particles move in stringlike sequences, is a phenomenon well studied in glassy materials [33–35] that has also been observed in particles at grain boundaries of colloidal crystals [36]. Here we observe cooperative particle motion during granule rotation. This is similar to the previously observed cooperative motion at grain boundaries, but here we find that the underlying moiré pattern directs the stringlike particle displacements so that they trace out the edges of the hexagonal granules.

Following [36], to identify cooperative motion we focus on the particles with the top 0.5% largest displacements over a set time period ($\Delta t = 180$ s). We find that during granule rotation, these particles move cooperatively in stringlike displacement sequences in which one particle moves out of its position and is replaced by another particle at the end of the time interval. We identify pairs of particles within a sequence as those for which the initial position of the first particle is the same as the final position of the second particle within an uncertainty of 60% of a particle diameter D. That is, particles are linked into the same stringlike cooperative rearrangement sequence if $|\vec{r}_1(t=0) - \vec{r}_2(t=\Delta t)| < 0.6D$. Notably, we find that the strings show a spatial pattern that follows the edges of the hexagonal vortices [Fig. 5(a)]. Thus, unlike the random particle strings observed in [36], here the cooperative motion is directed by the geometry of the underlying moiré pattern.

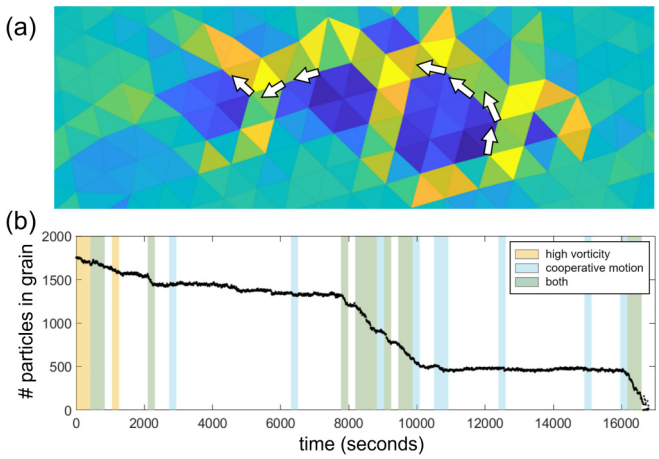

FIG. 5. Particles move cooperatively during granule rotation. (a) During a period of rapid grain dissolution, granules rotate, and the particles with the top 5% largest displacements (white arrows) move in cooperative motion strings along the edges of the hexagons defined by the underlying moiré pattern. (b) Time intervals that are characterized by *both* high vorticity and cooperative strings in colloidal particle motion indicate hexagonal granule rotation, and these correlate with periods of rapid grain dissolution.

To quantify the occurrence of cooperative motion during grain dissolution experiments, we count the number of particles moving in a stringlike sequence over each 180-s interval. In Fig. 5(b), intervals in which there are at least three particles moving in cooperative motion are highlighted with blue shading. Meanwhile, the yellow shading indicates intervals characterized by high vorticity, quantified as more than 5% of particle trios having vorticity higher than three times the standard deviation in vorticity. Intervals that have both significant vorticity and significant cooperative motion are highlighted with green shading. We note that the green-shaded regions faithfully track the regions with rapid grain dissolution, indicating that the observed periods of rapid dissolution occur via both cooperative motion and high vorticity. These are both signatures of hexagonal granule rotation.

VII. EFFECT OF LATTICE CONSTANT

Controlling the spacing between particles allows us to tune the grain dissolution mechanism: tightly packed crystals dissolve primarily via cooperative granule rotation, while looser

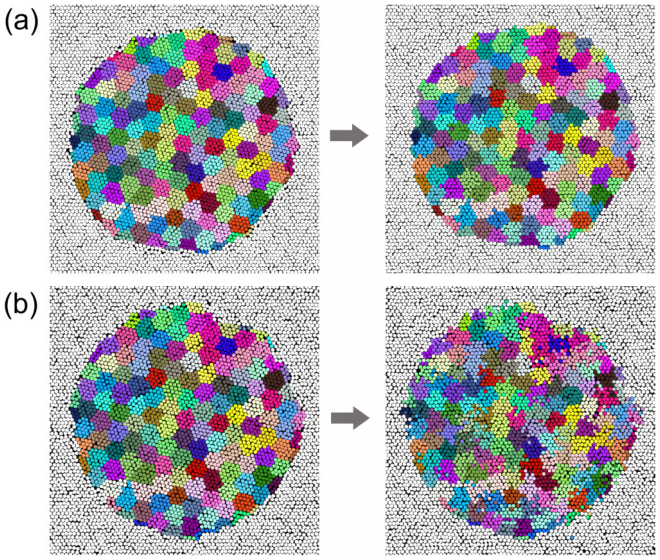

FIG. 6. Simulated crystals with higher lattice constants dissolve through random motion that is not coordinated into hexagonal granule rotation. For each panel, left is the initial particle configuration, and right is the final configuration after 20 000 simulation frames, once the embedded grain has completely dissolved. Particles are colored according to their initial moiré hexagon. The grain in (a) has a lattice constant of 1.05 particle diameters and shrinks primarily due to hexagon rotation, so the hexagonal regions retain their shape in the final particle configuration. The grain in (b) has a lattice constant of 1.08 particle diameters, and many particles move in random diffusive motion rather than rotating in cooperative granules. Consequently, the colors are scrambled in the final configuration.

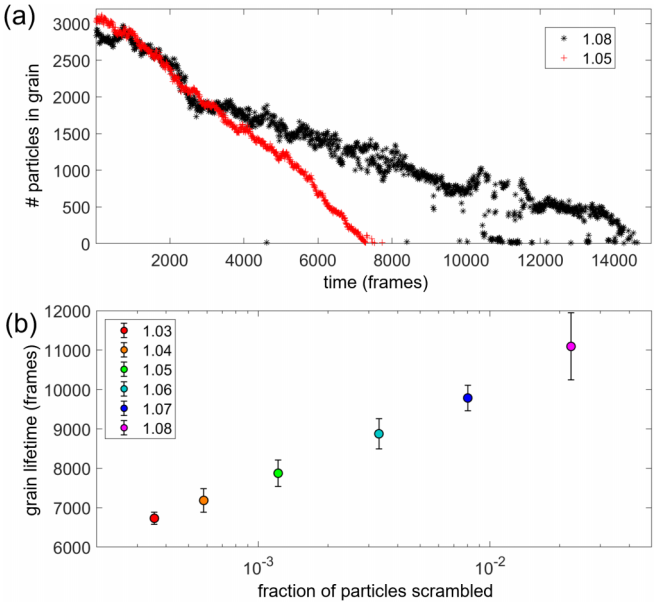

FIG. 7. Grain lifetime increases when fewer particles move in granule rotation. (a) The number of particles in the inner grain decreases more rapidly for the crystal with tighter particle spacing. This corresponds with a higher fraction of particles participating in hexagon rotation. (b) Grain lifetime is plotted against the fraction of particles that get scrambled into new moiré hexagons. Error bars indicate the standard error of the mean.

crystals allow more individual particle diffusion. We exploit this tendency to investigate how the rate of grain dissolution is related to hexagonal granule rotation. To this end, we measure grain lifetimes in Brownian dynamics simulations with varied lattice constants from 1.03 to 1.08 times a particle diameter D. This corresponds to a range of 0.855–0.778 in particle area fraction. This overlaps the range observed in our colloidal experiments (see Supplemental Material, Table S1 [31]). For all simulations, a circular inner grain is initialized within a surrounding outer crystal grain, with misorientation angle $\phi = 12^\circ$. At higher area fractions, we observe that nearly all particle motion is restricted to granule rotations; at lower area fractions, particle motion is diffusive and does not follow hexagonal granule rotation (Fig. 6). To track the degree to which particle motion differs from granule rotations, we use the underlying moiré pattern to identify which hexagonal granule each particle initially lies in. Once the grain has completely dissolved, particles that only moved according to granule rotation remain located in the same hexagonal granule that they started in. Conversely, particles that moved by diffusive, random displacements that are not determined by granule rotation can end up "scrambled" into a new granule other than the one they started in. In Fig. 6 particles are colored according to their initial hexagon granule—panel (a) shows a tightly packed crystal simulation with lattice spacing of 1.05 particle diameters, in which nearly all particles remain situated in their initial granules, while panel (b) depicts a loosely packed crystal simulation with lattice spacing of 1.08 particle diameters, where more particles scrambled into new granules.

Interestingly, we find that the more tightly packed crystals in which particles move primarily in granule rotation dissolve much more quickly than those looser crystals in which more particles diffuse out of their original moiré hexagon and get scrambled into a new hexagon. That is, we observe that grain lifetime is correlated with the fraction of particles that get scrambled out of their initial granules during grain dissolution (Fig. 7). A table showing data for each simulation run is provided in the Supplemental Material, Table S2 [31]. This result from simulations aligns with our experimental observation that periods of faster dissolution are correlated with granule rotation in hexagonal vortices.

VIII. SEQUENTIAL MOTION DURING GRANULE ROTATION

Granule rotation dictated by the underlying moiré pattern has been observed previously during grain splitting, a very rapid process in which the granules rotate synchronously [10]. In such cases the free energy peaks during rotation, leading to a barrier that prevents grain splitting from occurring in all but very small crystal grains wedged between two neighboring grains with low misorientation angles [10]. This differs from the current observation of widespread granule rotation during the dissolution of a single inner grain embedded within a single outer grain. The key difference is that here the granules do not rotate simultaneously but instead proceed through sequential particle motion. Particles move in cooperative strings, advancing into the empty spaces left behind by other particles,

as shown in a colloidal experiment in the Supplemental Material, Video S1, and in a Brownian dynamics simulation in Video S2 [31].

Because granule rotation occurs through sequential particle motion, the free energy cost is significantly lower than what would be needed to rotate all the granules simultaneously. Following [10], the time evolution of the free energy can be determined by finding the area of the free space available to each particle. The free space is computed as $F = -k_B T \sum_i \ln \frac{v_i}{\pi (D/2)^2}$, where k_B is the Boltzmann constant, D is the particle diameter, and v_i is the area of free space available to the ith particle. Thus, free energy is lower when particles have more free space available to them on average. The sequential cooperative motions of particles during granule rotation avoid synchronous rotations that would compress the crystal, as shown in the Supplemental Material, Video S3 [31]. This reduced free energy cost indicates that granule rotation likely plays a frequent role in the normal motions of grain boundaries, unlike grain splitting, which is predicted to occur only in rare situations.

IX. DISCUSSION AND CONCLUSIONS

We have observed that the motion of grain boundaries during the dissolution of a single grain embedded within a surrounding crystal is described by a combination of a slow mechanism characterized by random particle motions and a faster granule rotation mechanism in which particles move cooperatively in hexagonal vortices. The shape and placement of the rotating granules is determined by the underlying moiré pattern of the lattices of the inner and outer crystal grains. We find that during granule rotation, strings of cooperatively moving particles follow the edges of the rotating granules, which is distinct from previously observed random cooperative motion at grain boundaries [36]. This organized cooperative motion is reminiscent of the polygonlike cooperative rearrangements recently observed in "avalanche-driven" grain boundary diffusion [37].

Future studies of fluctuations of grain boundaries could determine whether this mechanism also occurs in situations where there is not a single grain boundary loop surrounding an inner grain. Incorporation of granule rotation into models for grain coarsening could help provide more accurate predictions for how self-assembled crystals age. Furthermore, since similar vortices have been observed in crystals composed of active rather than thermal particles [38], this mechanism could occur broadly in many polycrystalline systems across scales and across diverse energy sources.

ACKNOWLEDGMENT

This work was funded by the Research Corporation for Science Advancement through a Cottrell Scholar Award to S.J.G.

[1] M. Meyers, A. Mishra, and D. Benson, Prog. Mater. Sci. **51**, 427 (2006).
[2] K. Kreuer, Annu. Rev. Mater. Res. **33**, 333 (2003).
[3] P. Y. Huang, C. S. Ruiz-Vargas, A. M. van der Zande, W. S. Whitney, M. P. Levendorf, J. W. Kevek, S. Garg, J. S. Alden, C. J. Hustedt, Y. Zhu, J. Park, P. L. McEuen, and D. A. Muller, Nature (London) **469**, 389 (2011).
[4] T. O. E. Skinner, D. G. A. L. Aarts, and R. P. A. Dullens, Phys. Rev. Lett. **105**, 168301 (2010).
[5] S. Gokhale, K. H. Nagamanasa, R. Ganapathy, and A. K. Sood, Soft Matter **9**, 6634 (2013).
[6] Q. H. Wei and X. L. Wu, Phys. Rev. E **70**, 020401(R) (2004).
[7] I. Buttinoni, M. Steinacher, H. T. Spanke, J. Pokki, S. Bahmann, B. Nelson, G. Foffi, and L. Isa, Phys. Rev. E **95**, 012610 (2017).
[8] W. T. M. Irvine, A. D. Hollingsworth, D. G. Grier, and P. M. Chaikin, Proc. Natl. Acad. Sci. USA **110**, 15544 (2013).
[9] F. A. Lavergne, A. Curran, D. G. A. L. Aarts, and R. P. A. Dullens, Proc. Natl. Acad. Sci. USA **115**, 6922 (2018).
[10] A. R. Barth, M. H. Martinez, C. E. Payne, C. G. Couto, I. J. Quintas, I. Soncharoen, N. M. Brown, E. J. Weissler, and S. J. Gerbode, Phys. Rev. E **104**, L052601 (2021).
[11] W. T. Read and W. Shockley, Phys. Rev. **78**, 275 (1950).
[12] W. W. Mullins, J. Appl. Phys. **27**, 900 (1956).
[13] J. von Neumann, *Metal Interfaces* (ASM, Cleveland, OH, 1952), p. 109.
[14] C. Zener and C. Smith, Trans. AIME **175**, 15 (1948).
[15] A. Lobkovsky, A. Karma, M. Mendelev, M. Haataja, and D. Srolovitz, Acta Mater. **52**, 285 (2004).
[16] G. Gottstein, A. Rollett, and L. Shvindlerman, Scr. Mater. **51**, 611 (2004).
[17] Z. T. Trautt, M. Upmanyu, and A. Karma, Science **314**, 632 (2006).
[18] J. Hu, X. Wang, J. Zhang, J. Luo, Z. Zhang, and Z. Shen, J. Materiomics **7**, 1007 (2021).
[19] S. Okita and Y. Shibuta, ISIJ Int. **56**, 2199 (2016).
[20] J. Li, J. Appl. Phys. **33**, 2958 (1962).
[21] U. Erb and H. Gleiter, Scr. Metall. **13**, 61 (1979).
[22] J. W. Cahn and J. E. Taylor, Acta Mater. **52**, 4887 (2004).
[23] Z. T. Trautt and Y. Mishin, Acta Mater. **60**, 2407 (2012).
[24] M. Upmanyu, D. Srolovitz, A. Lobkovsky, J. Warren, and W. Carter, Acta Mater. **54**, 1707 (2006).
[25] D. Moldovan, V. Yamakov, D. Wolf, and S. R. Phillpot, Phys. Rev. Lett. **89**, 206101 (2002).
[26] S. Srinivasan and J. Cahn, Challenging some free-energy reduction criteria for grain growth, in *Science and Technology of Interfaces* (John Wiley & Sons Ltd., New York, 2002), pp. 1–14.
[27] F. A. Lavergne, A. Curran, D. G. A. L. Aarts, and R. P. A. Dullens, Eur. Phys. J. B **92**, 142 (2019).
[28] S. J. Gerbode, S. H. Lee, C. M. Liddell, and I. Cohen, Phys. Rev. Lett. **101**, 058302 (2008).
[29] C. E. Cash, J. Wang, M. M. Martirossyan, B. K. Ludlow, A. E. Baptista, N. M. Brown, E. J. Weissler, J. Abacousnac, and S. J. Gerbode, Phys. Rev. Lett. **120**, 018002 (2018).
[30] B. I. Halperin and D. R. Nelson, Phys. Rev. Lett. **41**, 121 (1978).

[31] See Supplemental Material at http://link.aps.org/supplemental/10.1103/PhysRevE.110.014608 for experiment and simulation data tables, as well as supplemental videos and figures.
[32] E. Bililign, F. Balboa Usabiaga, Y. Ganan, A. Poncet, V. Soni, S. Magkiriadou, M. Shelley, D. Bartolo, and W. Irvine, Nat. Phys. **18**, 212 (2022).
[33] E. R. Weeks, J. C. Crocker, A. C. Levitt, A. Schofield, and D. A. Weitz, Science **287**, 627 (2000).
[34] C. Donati, J. F. Douglas, W. Kob, S. J. Plimpton, P. H. Poole, and P. C. Glotzer, Phys. Rev. Lett. **80**, 2338 (1998).
[35] H. Zhang, D. J. Srolovitz, J. F. Douglas, and J. A. Warren, Proc. Natl. Acad. Sci. USA **106**, 7735 (2009).
[36] K. H. Nagamanasa, S. Gokhale, R. Ganapathy, and A. K. Sood, Proc. Natl. Acad. Sci. USA **108**, 11323 (2011).
[37] I. Chesser and Y. Mishin, Commun. Mater. **3**, 90 (2023).
[38] J. Menath, R. Mohammadi, J. C. Grauer, C. Deters, M. Böhm, B. Liebchen, L. M. C. Janssen, H. Löwen, and N. Vogel, Adv. Mater. **35**, 2206593 (2023).